

Article

Passive Structural Control on Skarn Mineralization Localization: A Case Study from the Variscan Rosas Shear Zone (SW Sardinia, Italy)

Fabrizio Cocco , Antonio Attardi, Matteo Luca Deidda, Dario Fancello, Antonio Funedda  and Stefano Naitza 

Department of Chemical and Geological Sciences, University of Cagliari, Cittadella Universitaria, S.S. 554 Bivio per Sestu, Monserrato, 09042 Cagliari, Italy; antatt94@gmail.com (A.A.); deiddam.geo@gmail.com (M.L.D.); dario.fancello@unica.it (D.F.); afunedda@unica.it (A.F.); snaitza@unica.it (S.N.)

* Correspondence: fabrcocco@unica.it

Abstract: The case study presented here deals with the Pb-Zn-Cu skarn ores hosted in the Rosas Shear Zone (RSZ), a highly strained domain located in the external zone of the Sardinian Variscan chain. The RSZ is characterized by several tectonic slices of Cambrian limestones within a strongly folded and foliated Cambrian-Ordovician siliciclastic succession, intruded by late Variscan granites and mafic dykes. Based on geological mapping, structural and microscope analyses, our results show that the skarn ores in the RSZ are an example of passive structurally controlled mineralization. The RSZ was structured close to the brittle–ductile transition and, once exhumed to shallower crustal levels, acted as plumbing system favoring a large-scale granite-related fluid circulation. The paragenesis and the mineralization style of the skarn vary slightly according to the peculiarity of the local structural setting: a tectonic slice adjacent to the mafic dyke; an intensely sheared zone or a discrete thrust surface.

Keywords: tectonic slices; mineralization; polydeformed basement; fluid circulation; brittle–ductile transition; mafic intrusion; thermal metamorphism; exhumation; metasomatism



Citation: Cocco, F.; Attardi, A.; Deidda, M.L.; Fancello, D.; Funedda, A.; Naitza, S. Passive Structural Control on Skarn Mineralization Localization: A Case Study from the Variscan Rosas Shear Zone (SW Sardinia, Italy). *Minerals* **2022**, *12*, 272. <https://doi.org/10.3390/min12020272>

Academic Editors: Huan Li and Han Zheng

Received: 19 January 2022

Accepted: 18 February 2022

Published: 21 February 2022

Publisher's Note: MDPI stays neutral with regard to jurisdictional claims in published maps and institutional affiliations.



Copyright: © 2022 by the authors. Licensee MDPI, Basel, Switzerland. This article is an open access article distributed under the terms and conditions of the Creative Commons Attribution (CC BY) license (<https://creativecommons.org/licenses/by/4.0/>).

1. Introduction

A proper identification, quantification and exploitation of ore deposits cannot be separated from a full comprehension of the structural control of the mineralization processes. This is particularly relevant for ores hosted in polydeformed basements, where the complexity of the structural setting is emphasized by the superposition of several deformation phases. Structural controls are critical in the genesis of hydrothermal ore deposits [1]. They define the pattern, extension, and modalities of the fluid flow in crustal sectors affected by mineralizing phenomena [2–4], not only determining the emplacement mode and the geometric–dimensional aspects of the deposits, but also influencing the type of fluid–rock interactions and the chemical mechanisms that determine the compositional characters of the ores [5,6]. The tectonic regime in which the mineralizing phenomena occur determines the prevalence of (1) passive controls, in which a frequently multi-scale network of pre-existing structural discontinuities in the host rocks forms a pre-established plumbing system for circulation and entrapment of hydrothermal fluids [7,8], or (2) active controls, in which deformation of rocks and development of the structural pattern is synchronous with the emplacement of mineralized deposits and is influenced by them [8–14]. In the framework of complex structures such as polyphasic shear zones, the two control modalities can repeatedly occur in several moments, but they are frequently related to dominantly extensional regimes [7]. This view assumes a particular declination in the case of districts characterized by skarn metasomatic deposits, in which (1) magma inflow and fluid circulations are favored by opening of pathways in large scale shear zones; (2) shear zone

structural set-up through tectonic slicing and cataclastic/mylonitic zones development results in a definite control on the spatial distribution and extension of reactive lithologies (e.g., carbonate rocks), susceptible to metasomatic phenomena and ore mineralization [15].

This study is focused on the Rosas Shear zone (RSZ), in the Sulcis subregion of SW Sardinia, which is considered as a key area in the definition of deformation styles at the crustal brittle–ductile transition in the south Variscan Sardinian chain [16], but it is also relevant for ore deposits studies, as home to a historical district (Rosas mine district) marked by widespread Pb-Zn-Cu mineralized skarns. Skarn ores are located along a complex pattern of tectonic slices and brittle structures enclosed in the RSZ and related to early Permian mafic and felsic magmatic pulses associated with the emplacement of the Sulcis pluton [17]. In this study, new structural field surveys and new studies on the ore deposits were performed to investigate the relationships between the geometry and evolution of the RSZ and late Variscan magmatic and metallogenic events, highlighting the role of structural passive control in the localization of the ore deposits in the Rosas district.

2. Geological Background

The segment of the south European Variscan chain exposed in Sardinia arose from the early Carboniferous continental collision and consists of three main tectono-metamorphic zones [18] (Figure 1a): an External zone in southwestern Sardinia, a Nappe zone in south-eastern and central Sardinia, and an Axial zone in northern Sardinia. During the Variscan collision, a Barrovian-type metamorphism developed increasing northward from very low grade in the External zone, to greenschist facies in the Nappe zone, to high grade in the Axial zone ([19], and references therein). The nappes were stacked with a top-to-the-south transport direction with the exception of the uppermost tectonic unit that was thrust over the External zone with a top-to-the-west transport direction [20,21]. During the late Carboniferous-Permian, the Variscan chain was involved in the post-collisional extension, and the Sardinian basement was affected by low- and high-angle normal faults [22]. At the same time, the emplacement of the Variscan granitoids occurred, leading to HT-LP metamorphism development [23,24].

The RSZ (Figure 1b,c) is part of the External zone located at the footwall of the Arburese thrust, the regional structure that separates the Variscan External zone from the Variscan Nappe zone [25] (Figure 1b).

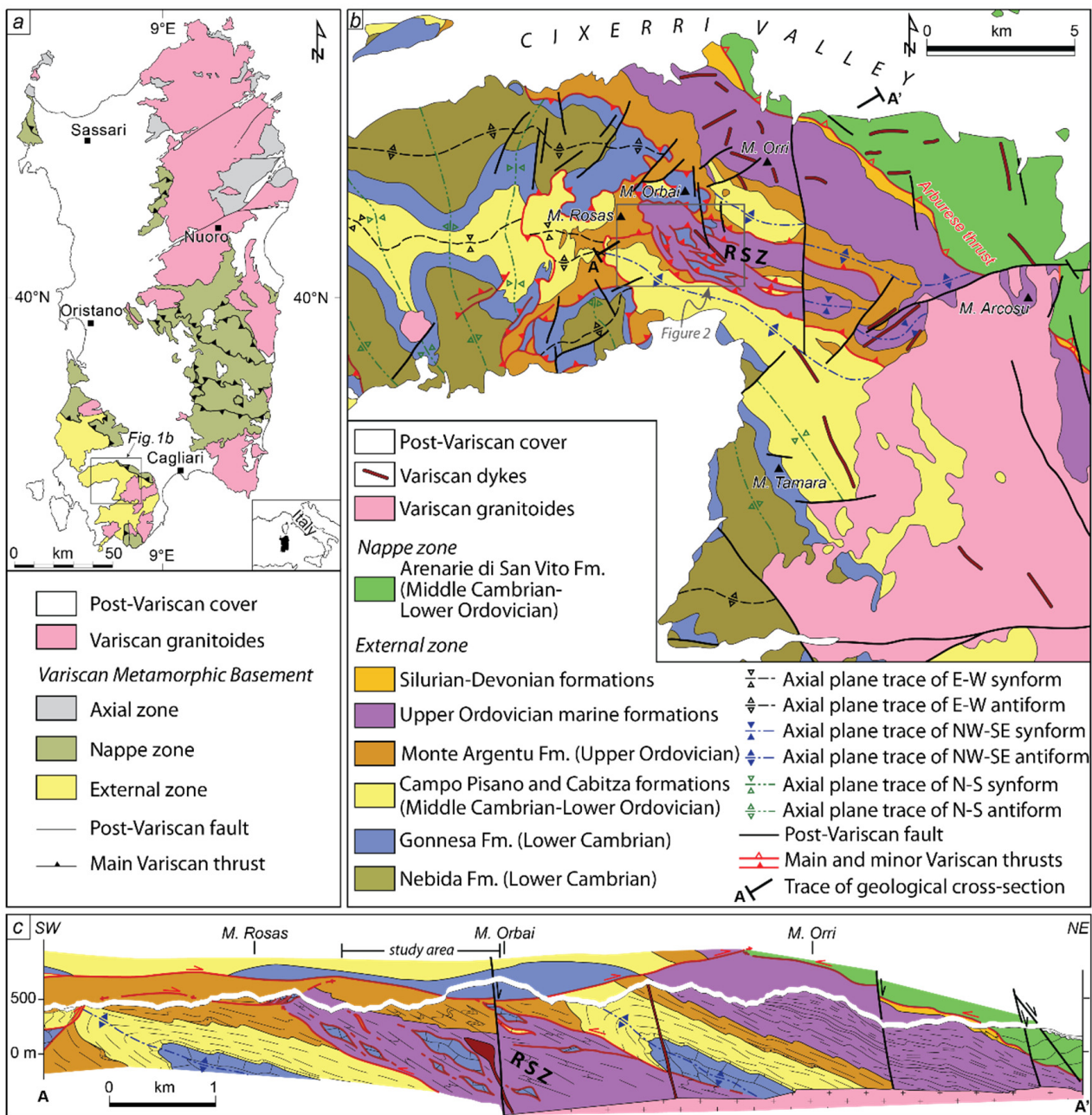


Figure 1. (a) Tectonic sketch map of the Variscan basement of Sardinia (after [26]); (b) geological sketch map of the central sector of the external zone. Location in Figure 1a. RSZ: Rosas Shear Zone. The grey box shows the location of Figure 2. (c) Geological cross-section across the Rosas Shear Zone (after [25]).

2.1. Stratigraphic Setting

The stratigraphic succession of the External zone is subdivided into two mega-sequences separated by a regional angular unconformity (Sardic Unconformity; [27]) ascribed to the Sardic Phase [28], a tectonic event related to the geodynamic processes affecting the northwestern Gondwana margin in Ordovician times [29–32].

The pre-Sardic sequence spans in age from lower Cambrian to lower Ordovician and consists of the following formations [33]: the Nebida Fm. (lower Cambrian), a 500 m thick siliciclastic succession characterized by alternating layers of sandstones and siltstones and by the occurrence of a continuous oolite level and episodic limestone intercalations; the Gonnese Fm. (lower Cambrian), an up to 500 m thick carbonate succession mainly

made up of well-stratified dolostones and massive limestones [34]; the Campo Pisano Fm. (middle Cambrian), a 20–50 m thick succession of alternating claystones and marly limestones [35]; the Cabitza Fm. (middle Cambrian-lower Ordovician), a 400 m thick siliciclastic succession characterized by alternating layers of claystones, siltstones and fine-grained sandstones [36].

The post-Sardic sequence starts with the Monte Argentu Fm. (upper Ordovician), a siliciclastic succession highly variable in thickness, from few tens to hundreds of meters, characterized at the base by olistoliths, megabreccias and conglomerates followed up section by marine sandstones and siltstones [37]. The marine depositional environment persisted throughout the whole upper Ordovician, during which a sedimentary succession 600 m thick was deposited (Monte Orri Fm., Portixeddu Fm., Domusnovas Fm. and Rio San Marco Fm.; [38]). Finally, the younger formations involved in the Variscan deformation are the Genna Muxerru, Fluminimaggiore, and Mason Porcus fms (Silurian-Devonian in age), mainly characterized by black-shales and limestones [39], and the Pala Manna Fm. (lower Carboniferous) characterized by clastic deposits [40].

The lower Cambrian-lower Carboniferous succession was intruded during lower Permian by numerous granitoid bodies and associated mafic and felsic dikes forming the Sulcis pluton [17] that crops out few kilometers to the SE of the RSZ (Figure 1b) and most likely occurs at shallow depth beneath the Rosas mine district (Figure 1c). In southern Sardinia, the intrusion of mafic dykes is a process that lasted for a long time span, more than 10 Ma, so dykes may pre-date, be coeval or post-date the granite body intrusion [17,41]. The outermost part of the Pluton in Northern Sulcis consists of F-bearing, ferroan ilmenite-series, subaluminous I-type granites (“GS1 suite”, [17]), dated at 289 ± 1 Ma by Re-Os on molybdenite [42]. Siderophyllitic dark mica (the only mafic mineral) and ilmenite, xenotime-Y and fluorite accessory minerals are distinctive of the GS1 granites, which also keep a significant metallogenic potential, being related to many W-Sn-Mo hydrothermal deposits in southern Sardinia [43,44].

2.2. Structural Setting

The Variscan External zone suffered three main shortening events that gave rise to a fold-and-thrust belt with a complex structural setting characterized by superposed folds, fore-thrusts and back-thrusts [45–47].

The lower Cambrian-lower Ordovician sedimentary succession was affected by a compressional event related to the Sardic Phase during which E-trending folds originated according to a N-S shortening direction. The Sardic folds have a kilometric wavelength, upright axial surface without any related tectonic foliation, and close tightness, as testified by the limbs cut by the Sardic unconformity with an angle approaching 90° . An important erosion affected the folded succession so that in several areas, the upper Ordovician sedimentary deposits lie just above the lower Cambrian sandstones and limestones of the Nebida and Gonnese fms. This mainly happens in the crest of the Sardic antiforms, whereas in the hinge zone of the synforms, the lower Ordovician siliciclastic succession of the Cabitza Fm. is usually preserved [48,49].

In Carboniferous time, the entire lower Cambrian-lower Carboniferous stratigraphic succession was involved in the deformation related to the Variscan Orogeny. During the first Variscan Phase, the N-S shortening direction caused E-trending open folds that gently deformed the post-Sardic Unconformity succession and that superposed in parallel on the Sardic folds. During the second Variscan Phase, the shortening direction progressively rotated from NE–SW to E–W, originating in sequence SW-facing overturned folds and the RSZ with a top-to-the-SW transport direction, W-facing folds with a well-developed axial plane foliation, W-verging fore-thrusts and, finally, E-verging back-thrusts and E-facing back-folds [25]. The superimposition of ductile and brittle structures related to different shortening directions results in a very complex stratigraphic structural setting in which the strain partitioning separates domains of very high strain intensity from others where

the intensity of the deformation is so low that the primary characteristics of the rocks, as bedding and sedimentary structures, are fully preserved.

The RSZ is a highly strained domain consisting of a 1 km thick shear zone located few kilometers westward of the leading edge of the Nappe front. It dips toward NE and lies beneath and subparallel to the Arburese thrust. The RSZ is bounded by two thrusts that developed along the limbs of two km-scale overturned antiforms that affect the lower Cambrian-upper Ordovician succession showing a SW-facing direction [25] (Figure 1b,c). A detailed description of the complex internal structure of the RSZ and the deformation processes along with its relationships with the ore mineralization will be provided in the next paragraphs.

3. Ore Deposits of the Sulcis Area

The SW of Sardinia has been one of the most important Zn-Pb-Ag mining districts of Europe with a peak of activity during the 19th century. The northern side of the district, the Iglesias area, hosts several giant and high-grade MVT and SEDEX Zn-Pb-Fe deposits such as those exploited in the old mines of Monteponi, San Giovanni, Masua, Nebida, Monte Agruxiau, San Benedetto, Campo Pisano, Genna Luas. These deposits consist of stratabound and discordant orebodies with variable proportions of Cd-rich sphalerite, Ag-rich galena and pyrite which formed in the carbonate platform, represented by the Gonnese Formation, during Cambrian extensional tectonics [47,50]. Conversely, in the Sulcis area, the southern side of the district, skarn deposits are a frequent typology. They are genetically and spatially related with the emplacement of the GS1 suite granites and to the strong hydrothermal activity generated from intrusive bodies, which produced the aforementioned W-Sn-Mo (\pm Fe-Pb-Zn-Cu-As-F-Bi) distinctive metallogenic association. Accordingly, the mineral expression of this geochemical footprint in skarns of SW Sardinia is represented by massive magnetite-fluorite and Cu-Zn-As-Fe-Pb sulfide orebodies with, most importantly, variable concentrations of cassiterite, scheelite, Bi-Pb-Ag-sulfosalts, stannite and molybdenite. Some of these indicative minerals have been reported in various localities of SW Sardinia [44]: most notably, the occurrence of scheelite have been reported in samples from the Sa Marchesa and Monte Tamara mining areas of Sulcis [51–53], 2–10 km south from the Rosas mine area. These skarn orebodies are small in size but numerous and recurrently located along tectonic contacts, thrusts and fractures both in the carbonate rocks (Gonnese and Campo Pisano fms.) and at the contacts between carbonate and siliciclastic rocks (Nebida Fm. at the base and of Cabitza Fm. at the top). In many cases, as in the Monte Tamara area, faults appear to have provided a permeability pattern that favored the extent of hydrothermal fluids circulation in rocks and a broader development of metasomatic processes. Therefore, size and geometry of skarn orebodies, their mineral zonation and their extension at depth are controlled by these structures. These assumptions could also be extended to the more intensely deformed structural setting of the Rosas mine area (Figure 2).

The Rosas mine, active from the 19th century to the 1980s, was one of the most important of Sulcis region and comprised numerous mine workings throughout an area of roughly 6 km². Among the different mineralized bodies occurring in this area, several skarn ores were exploited extensively for their Zn-Pb sulfide contents in the mine workings of Barisonis, Mitza Sermentus, S'Ega Fogus, S'Ega Su Forru, Truba Niedda (Figure 2). Bechstadt and Boni (1994) [34] proposed an Ordovician age for the whole stratigraphic sequence, including the limestones. In more recent studies, various authors [16,25,54] interpreted the limestones as belonging to deformed portions of the lower Cambrian Gonnese Fm. enclosed inside the complex pattern of tectonic slices of RSZ, prevalently comprising elements from the upper Ordovician sequence. Indeed, the arrangement of metasomatized limestones along the NW–SE alignment of the main RSZ structure suggests a more effective structural control compared to other Sulcis areas where deformations and structural outlines are not as pervasive. Moreover, along the prosecution of the RSZ to the SE in the Campanasissa locality, other skarns are mentioned [55] close to

the contact with the GS1 intrusion. Granitoids do not crop out in the Rosas area, but their occurrence at shallow depth beneath the Rosas mine district is suggested by the widespread granite-related mineralization; Variscan magmatic rocks are represented by a swarm of mafic calc-alkaline dikes that intrude in the basement following the main tectonic lineaments, oriented NW–SE, of the RSZ. The most relevant magmatic body is a large gabbroid dike that crops out in the central part of the area, spatially associated with numerous orebodies (e.g., Barisonis mineworks) (Figure 2). For this reason, a genetic relationship between the gabbro and the skarn ores has been repeatedly inferred in the past when the mine was operating [56], but no clear evidences have been provided yet to verify this hypothesis. Cavinato (1937) [57] excluded these relationships based on considerations on skarn paragenesis and the relatively small volume of basic magmas in the area. Anyhow, the relationships between the developing of the main tectonic structures, the emplacement of the gabbro and the formation of the skarn orebodies have been further detailed in this study, in the three key areas of Barisonis, Mitza Sermentus and S'Ega Su Forru (Figure 2).

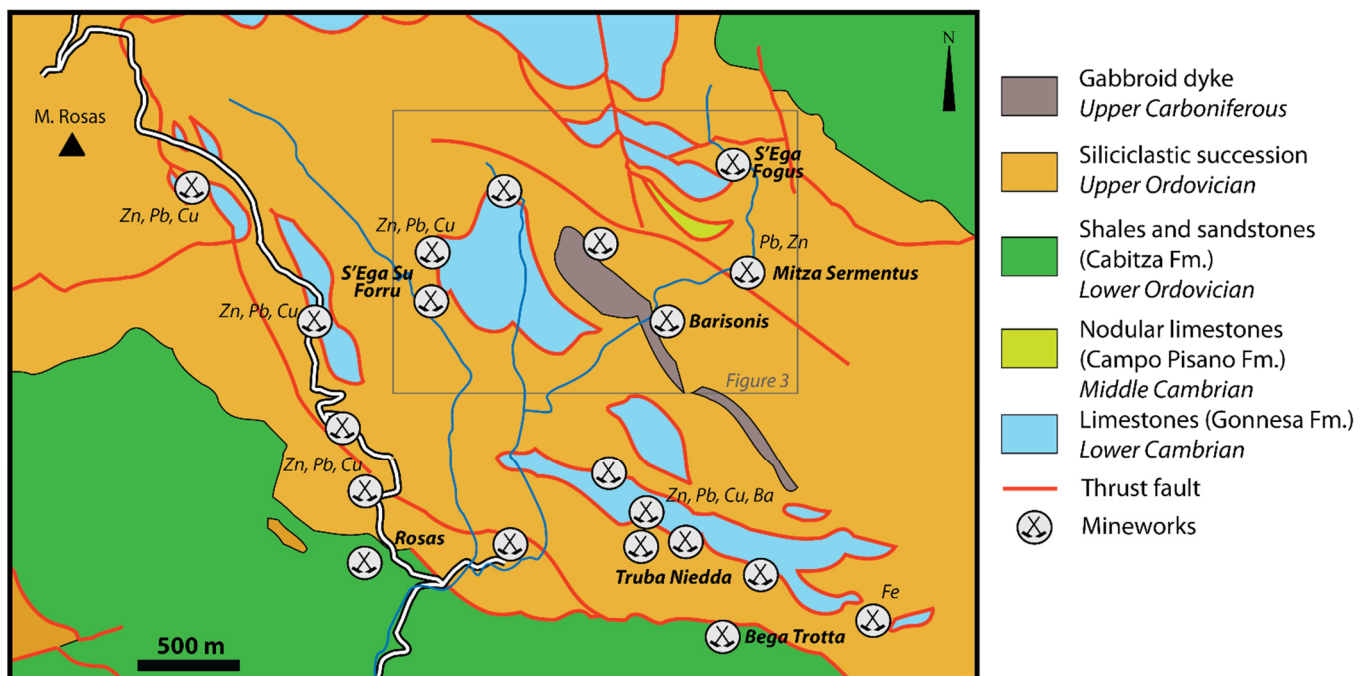


Figure 2. Geological sketch map (after [58]) and main mineworks in the Rosas district (after [54,59], modified). Location in Figure 1. The grey box shows the location of the study area in Figure 3.

4. Material and Methods

In order to infer which relationship exists between tectonic structures, magmatic intrusion and skarn ores, a geological and structural mapping at 1:5000 scale has been performed, starting from the geological map at 1:50,000 scale “Foglio 556 Assemini” [58] carried out by the Italian Geological Survey (ISPRA Carg Project; [54]). The field investigation aimed to further detail the main stratigraphic and tectonic contacts and the structural features, as foliations, folds and kinematic indicators, paying special attention to the areas where the main skarn ores were exploited.

The geological map has been validated by structural contouring, following the procedure proposed by [60]. This procedure allowed us to check the consistency of the detected tectonic contacts and to project properly them in the geological cross-sections, providing a more accurate attitude of the thrusts.

Microstructural and petrographic analyses were carried out on representative samples from the areas of Barisonis, Mitza Sermentus and S'Ega Su Forru. Thin and polished sections were firstly observed at the Department of Chemical and Geological Sciences of

Cagliari, University of Cagliari, Monserrato, Italy, under transmitted and reflected light in Optical Microscopy (OM) with a JenaLab polarizing microscope; then, SEM-EDS analyses were performed on selected samples at CESAR laboratories of Università di Cagliari, using a Quanta Fei 200 unit equipped with a ThermoFischer Ultradry EDS detector operating under both low- and high-vacuum conditions, 25–30 KeV voltage and variable spot size.

5. The Rosas Shear Zone and Related Skarn Ores

5.1. Structure of the Rosas Shear Zone

The core of the RSZ, where the large part of the addressed skarn ores are located, shows a complex internal structure characterized by several anastomosing thrusts that bound map-scale tectonic slices derived from the Gonnesa, Campo Pisano, Cabitza and Rio San Marco fms. (Figure 3). Because of the intensity of the deformation, the lithostratigraphic attribution of the siliciclastic succession that wraps these tectonic slices is often difficult. However, interpreting the primary features preserved in less strained domains, the upper Ordovician Monte Orri and Monte Argentu fms have been recognized. This characterization also contributes to better define the structure of the RSZ, given information on the deformation style.

The Monte Argentu Fm. crops out in the northern sector of the study area and consists of alternating layers of conglomerates, sandstones and siltstones, where diagenetic nodules characterized by a maximum diameter of 1 cm and an elongate cigar shape occur. The Monte Orri Fm. crops out extensively in the southern sector of the study area and is mainly made up of alternating sandstones and siltstones. The stratigraphic polarity is frequently reversed because of the thrusting and also of the occurrence of large overturned folds (Figure 1c). The main feature at the outcrop scale in the siliciclastic formations is a penetrative NE-dipping cleavage along which the original bedding is transposed, although in some cases it is still possible to recognize the bedding attitude by means of chromatic and grain size variations. In this last case, isoclinal folds with NW-striking axis and NE-dipping axial plane can be identified. At micro-scale, the tectonic foliation varies from disjunctive to slaty cleavage, depending on grain size. In the higher strained zones, mm-size quartz porphyroclasts show asymmetrical sigma shapes consistent with a top-to-the-SW transport direction.

Among the others, the tectonic slices belonging to the Gonnesa Fm. are the most relevant for this study because they host the skarn ores. These slices are embedded in both the Monte Argentu and Monte Orri fms and are mainly made up of gray to black massive limestones. The thrusts that bound the slices dip towards N–NE, with the top thrust generally steeper than the bottom thrust (Figure 3). The size of the slices is highly variable, ranging in length from 1 to 100 m and reaching the maximum thickness of 100 m. For instance, in the Barisonis and Mitza Sermentus mines the limestone slices are very small, only few meters thick, whereas the skarn in the S'Ega Su Forru mine is hosted in a slice more than 150 m thick (Figure 3). Contact metamorphism and sulfide disseminations on the limestones are evident in the proximity of the tectonic contacts in many cases accompanied by 1-m-thick quartz veins in the terrigenous formations. At the micro-scale, calcite shows grain size reduction and a dynamic recrystallization, leading to fine-grained calc-mylonites where asymmetric grains oblique to the main foliation reveals a top-to-the-SW sense of shear that is the same inferred from the kinematic indicators detected in the siliciclastic formations.

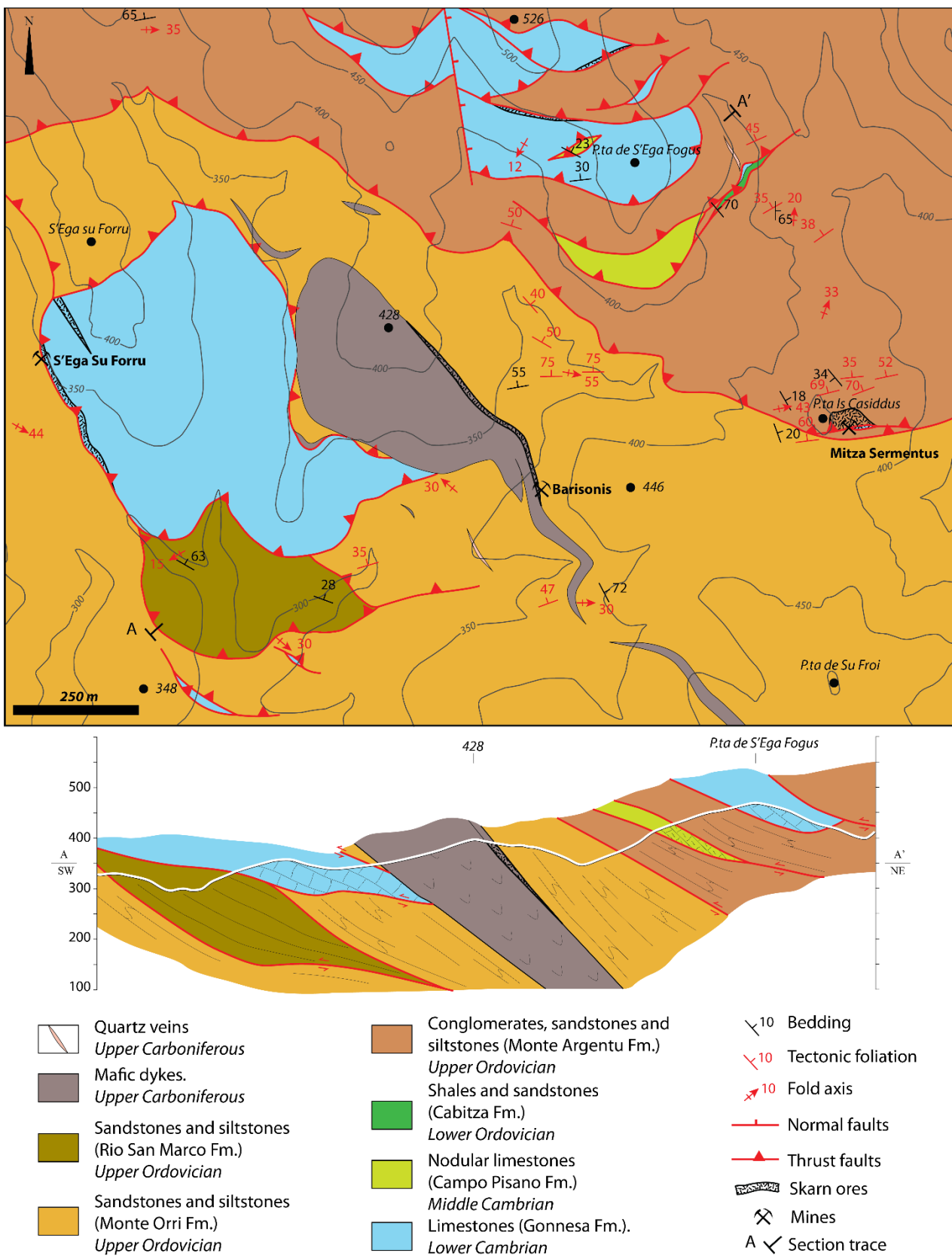


Figure 3. Geological map of the Rosas Shear Zone and geological cross-section. Location in Figure 2. Note that the limestone slices in the Barisonis and Mitza Sermentus mines are very small and have not been drawn at the scale of this map.

The occurrence of tectonic slices derived from lower Cambrian to upper Ordovician formations provides evidence of a widespread tectonic shearing and a very high displacements accommodated by slip along the foliation surfaces. As suggested by Casini et al. (2010) [16], the active behavior of the tectonic foliation is facilitated by the occurrence of detrital muscovite that, once passively rotated towards the cleavage plane, acted as microstructural lubricant favoring the sliding along each foliation plane, avoiding internal grain deformation. The main deformation mechanisms active in the RSZ include pressure solution, grain boundary sliding, deformation lamellae and mechanical twinning [16,25], suggesting that the RSZ structured near the crustal brittle–ductile transition, under sub-greenschist facies, in a depth range of 11.5–13.5 km and a temperature range of 250–300 °C [16,25]. The microstructures associated to the main foliation suggest that it must be considered as an active foliation along which part of the dislocation of the shear zone took place. A post-tectonic annealing, possibly related to the magmatic intrusion described in the follow, is reported.

The RSZ has been affected in late Carboniferous-Permian times by a gabbroid intrusion that consists of a main large mafic dike with a thickness of about 100 m and several smaller veins of metric thickness. The dike dips northeastward, subparallel to the main tectonic contacts, reaches its maximum width near Punta Atzori and thins towards SE. The top and bottom contact of the dike dip 60° and 40°, respectively, leading to a progressively thinning of the dike with depth. The whole gabbroid mass is crossed by cooling joints that dip of about 60° towards SW, perpendicular to the dike attitude. At the outcrop scale it shows a doleritic structure, dark green to dark gray in color, characterized by sub-millimetric amphibole (hornblende) and chlorite crystals. In thin section plagioclase (andesine), pyroxene (augite), hornblende, epidote, chlorite, calcite and muscovite are recognizable, arranged in ophitic texture that suggests a hypabyssal origin for the intrusion. Several minor mafic dikes, parallel to the gabbroid dyke, crop out discontinuously within the siliciclastic host rocks. The intrusion process seems to have been favored by the occurrence of the cleavage that has been exploited as surfaces of weakness by the dike swarm, although in some cases the tectonic foliation is cut across. This unequivocally demonstrates that the dyke intrusion post-dates the RSZ structuring.

5.2. Field Relationships of the Orebodies

In the following, we describe the field relationships of the orebodies in some of the most relevant mine works located in the study area, namely Barisonis, Mitza Sermentus and S'Ega su Forru (Figure 3).

5.2.1. Barisonis

The Barisonis mine site consists of a 10-m-wide stope with short galleries and dumps. The orebody is hosted in a metasomatized lens-shaped carbonate slice of the Gonnese Fm., embedded in the upper Ordovician siltstones of Monte Orri Fm. (Figure 4). On the main stope, the skarn measures 10 m in thickness and closes abruptly to the S. Although the presence of a steep dump limits its exposure at the N of the adit, the slice seemingly reduces in width and closes shortly thereafter. On the E contact, a 5–7 m thick gabbro dyke crops out between the skarn and the Monte Orri Fm. rocks. The skarn is dark green and with a visible zoning pattern represented by garnet, clinopyroxene and wollastonite bands parallel to the contacts with the gabbro and the siltstones (Figure 4). The garnet bands are mostly located at the edges of the skarn close to the host rocks. Clinopyroxene became prevalent on the garnet in a more internal zone, while wollastonite is more abundant in the inner part of the skarn. In terms of relative abundances, clinopyroxene appears as the main calc-silicate throughout the outcrop, locally forming decametric-size bands of dark green idiomorphic elongated crystals up to 5 cm in length. In the inner zones of the skarn, where calcite and quartz veins also appear, chlorite and amphibole broadly form at the expense of clinopyroxene bands. The sulfide ore hosted in the skarn consists of abundant sphalerite, chalcopyrite, galena and pyrite mostly concentrated in the upper garnet-clinopyroxene

bands. Secondary Cu-sulfides (covellite, bornite) pockets can be observed towards the inner wollastonite zone closer to the gabbro contact.

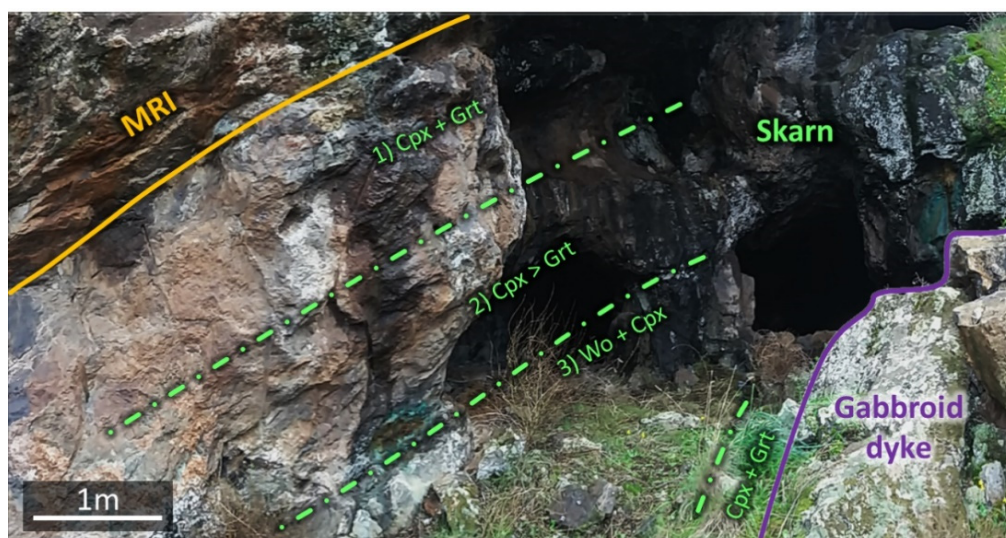


Figure 4. Lens-shaped skarn at the Barisonis mine embedded within the siliciclastic Monte Orri Fm. (MRI) and the gabbro dyke. The mineral zoning pattern is also shown.

5.2.2. Mitza Sermentus

The Mitza Sermentus old Zn-Pb mine is located on the Is Casiddu high, about 0.7 km east from Barisonis (Figure 3). It consists of a 130 m wide open pit and a 60–70 m deep system of underground levels. The main sulfide mineralization is hosted in irregular lens-shaped metasomatized carbonate slices embedded in dark shales belonging to the Monte Argentu Fm. (Figure 5). The slices display an E–W to ESE–WNW direction dipping 30–35° to the NNE. The orebodies size, extent of metasomatism and grade of mineralization increase from the top to the bottom of the pit. Small (up to 1.5 m) and barren to strongly oxidized shreds of calc-silicate hornfels prevail at the top of the sequence. Conversely, a higher grade 10 m thick massive skarn orebody is located at the bottom of the pit. The skarn features a light green color and a banded structure made of fine-grained wollastonite-clinopyroxene, epidote and chlorite. At the outcrop scale, a distinct zoning pattern is difficult to identify. Garnet occurs with small magnetite bands at the immediate contact with the shales in the upper part of the pit. Conversely, in the lower part of the pit, garnet and clinopyroxene are apparently subordinate with respect to wollastonite, and retrograde phases like epidote and chlorite are very abundant. The foremost ore minerals are here represented by chalcopyrite, sphalerite and galena with subordinate pyrite. They generally form cross-cutting veinlets, massive aggregates and disseminations in the calc-silicate gangue. The contact between the skarn and the siliciclastic formation is marked by a band of dark shales bleached and affected by intense hydrothermal alteration. Thus, a swarm of thin veinlets of chalcopyrite-sphalerite infill in the phyllites rock foliation. The veinlets are cm-scale and are often accompanied by a more competent white-greenish matrix. In the upper zone, small centimetric to decimetric arsenopyrite-pyrite lenses are emplaced along the shale foliation planes. Skarn veins also involve the mafic dikes intruding the dark shales, producing a further type of metasomatized and sulfide-mineralized rock.

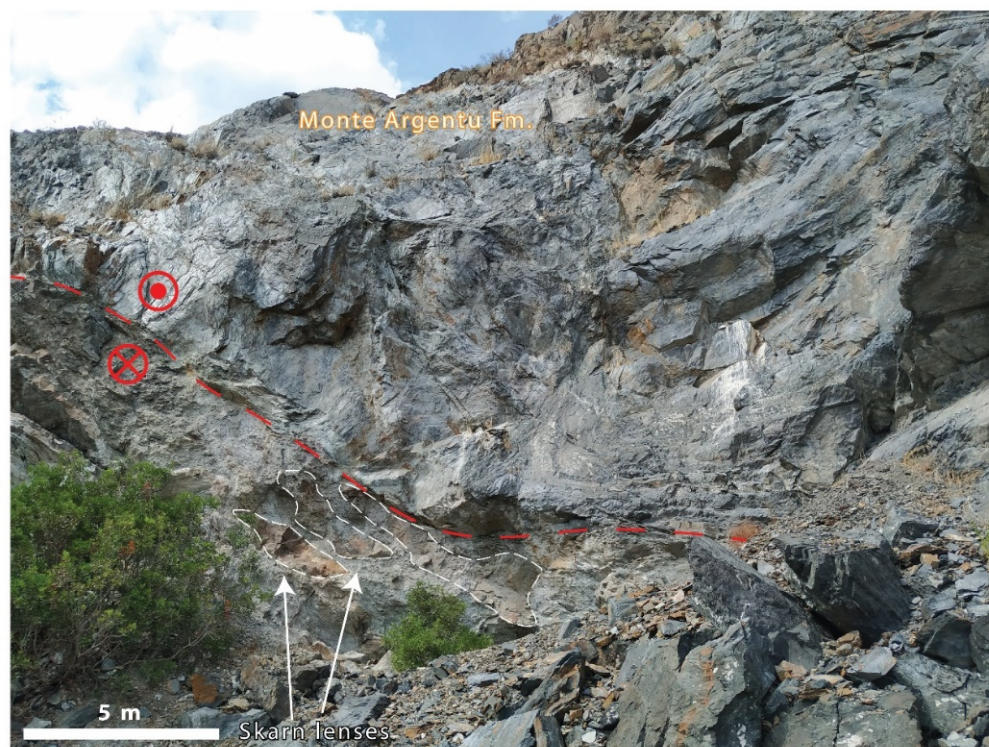


Figure 5. Lens-shaped skarn lenses at the Mitza Sermentus mine embedded in the shales of the Monte Argentu Fm; red dashed line: Variscan thrust with tectonic transport direction the-top-to-the-SW (view from SW).

5.2.3. S'Ega Su Forru

The S'Ega Su Forru old mining site is located roughly 1 km NW from Barisonis (Figure 3). In this locality, a series of small and today often inaccessible galleries are widespread along a large slice of partly metasomatized Cambrian limestones embedded in the upper Ordovician siltstones and sandstones of the Monte Orri Fm. Thermal recrystallization, suggested by the white and greyish-black banded texture, is widespread throughout the limestones. Moreover, traces of thin veinlets and nests of galena-chalcopyrite-pyrite are made particularly evident by the malachite-azurite alteration of chalcopyrite. The skarn orebodies of this locality are remarkably smaller in size compared to those from Barisonis and Mitza Sermentus. In fact, the main orebody consists of a 20 cm NNW–SSE dipping skarn vein ($N330-60^\circ$) formed at the tectonic contact between marbles and siltstones (Figure 6a,b). The skarn vein has a dark greenish-grey color and a fine-grained texture, seemingly dominated by retrograde calc-silicate minerals such as epidote, amphibole and chlorite. Sulfides, among which idiomorphic crystals of pyrite and galena are the most abundant, are disseminated in the gangue. Chalcopyrite is also present, showing a deep green malachite alteration. Moving downward along the same tectonic contact, the marbles are seemingly barren. Moreover, their color changes to a brownish and vuggy, more dolomitic facies.

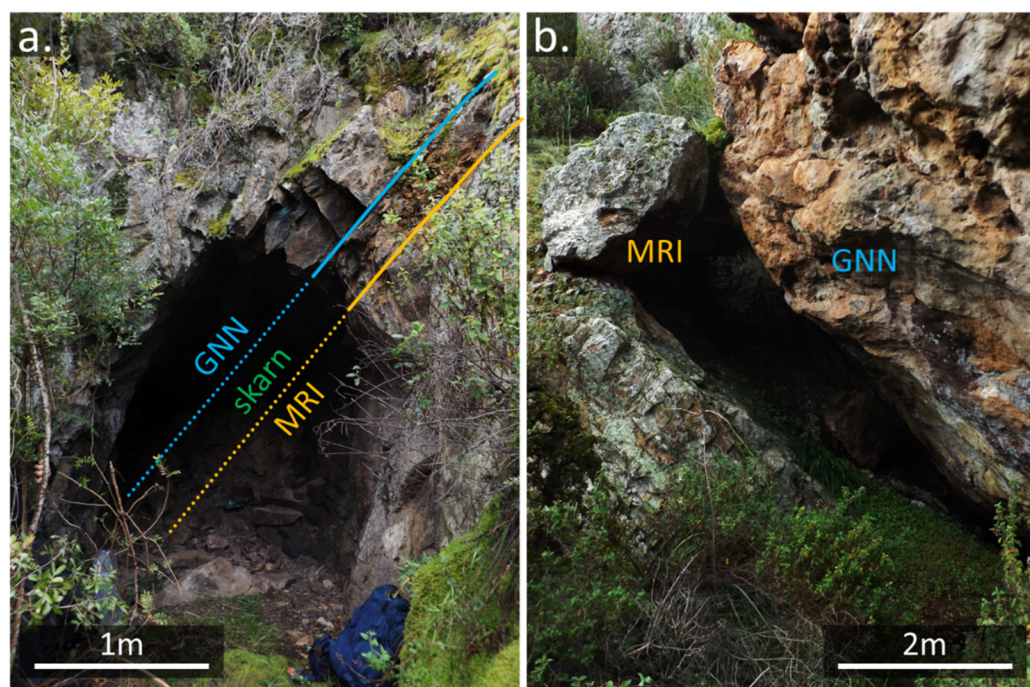


Figure 6. Relationships between the tectonic contact and the skarn mineralization at the S'Ega Su Forru locality. (a) thin skarn band (20 cm) located along the contact between a slice of recrystallized Cambrian limestone of the Gonnese Fm. (GNN) and Ordovician phyllites of the Monte Orri Fm. (MRI); (b) same contact of (a) in a lower stratigraphic position between phyllites and a more magnesian facies of the GNN, where no skarn ore has been detected.

6. Ore Microscopy and SEM-EDS Analyses

6.1. Barisonis

A total of 12 samples from Barisonis have been collected to further detail the mineral zoning of the skarn observed at the outcrop scale. The samples are representative of (a) the outer garnet zone (BS.S2.11; BS.S2.10; BS.S2.11); (b) the clinopyroxene zone (BS.S203); and (c) the inner wollastonite zone (BS.S2.04; BS.S2.05; BS.S2.06; BS.S2.08).

The mineralogy of the samples from Barisonis represents a well-developed calcsilicate assemblage. It is characterized by early wollastonite, clinopyroxene and garnets of the metasomatic, prograde stage followed by a retrograde hydrothermal alteration during which amphiboles, epidotes, chlorite, hematite and calcite were formed.

Garnets along the contacts with the wall rocks, namely the sandstones and the gabbro, form homogeneous bands of anhedral crystals. They are generally isotropic towards the core with birefringent rims (Figure 7a) that become more evident where the hydrothermal alteration is more advanced and retrograde calcsilicates (chlorite and amphiboles) develop at the edges of crystals and between the rims. From EDS analyses, their compositions range from almost pure andradite (Adr_{97}) to grossular-dominant ($\text{Grs}_{72-67}\text{Adr}_{24-27}$) with minor spessartine components (Sps_{1-3}). A transitional oscillatory zoning of alternating Fe-rich and Al-rich garnet is commonly found. Clinopyroxenes essentially belong to the hedenbergite term (14–16 wt.% of Fe and 0–3 wt.% of Mg) with appreciable manganese contents up to 5 wt.%. Amphiboles from the inner zone of the orebody fall in the field of the ferroactinolite-actinolite series (up to 20 wt.% Fe). Their composition is arguably inherited by the hedenbergitic clinopyroxene, more abundant than diopside. In fact, extensive substitution of amphiboles over clinopyroxene crystals is evident. Quartz and calcite are widespread and testify a strong carbonation of calc-silicate phases. Wollastonite, in particular, is completely substituted by needle-shaped quartz and very fine-grained calcite (Figure 7b). Millimeter-scale seams of massive chlorite are also typical of this zone, frequently enveloping sub-millimetric crystals of rutile with titanite reaction rims.

Conversely, rounded and “worm-like” chlorite aggregates with distinct blue birefringence are associated with magnetite and cassiterite veinlets in a quartz-fluorite gangue. Moreover, interstitial spatic calcite and quartz-fluorite veins and pockets occur in the lower-central parts of the outcrop. The mineralizing stages closes with the formation of quartz and calcite, cementing all the previously formed minerals.

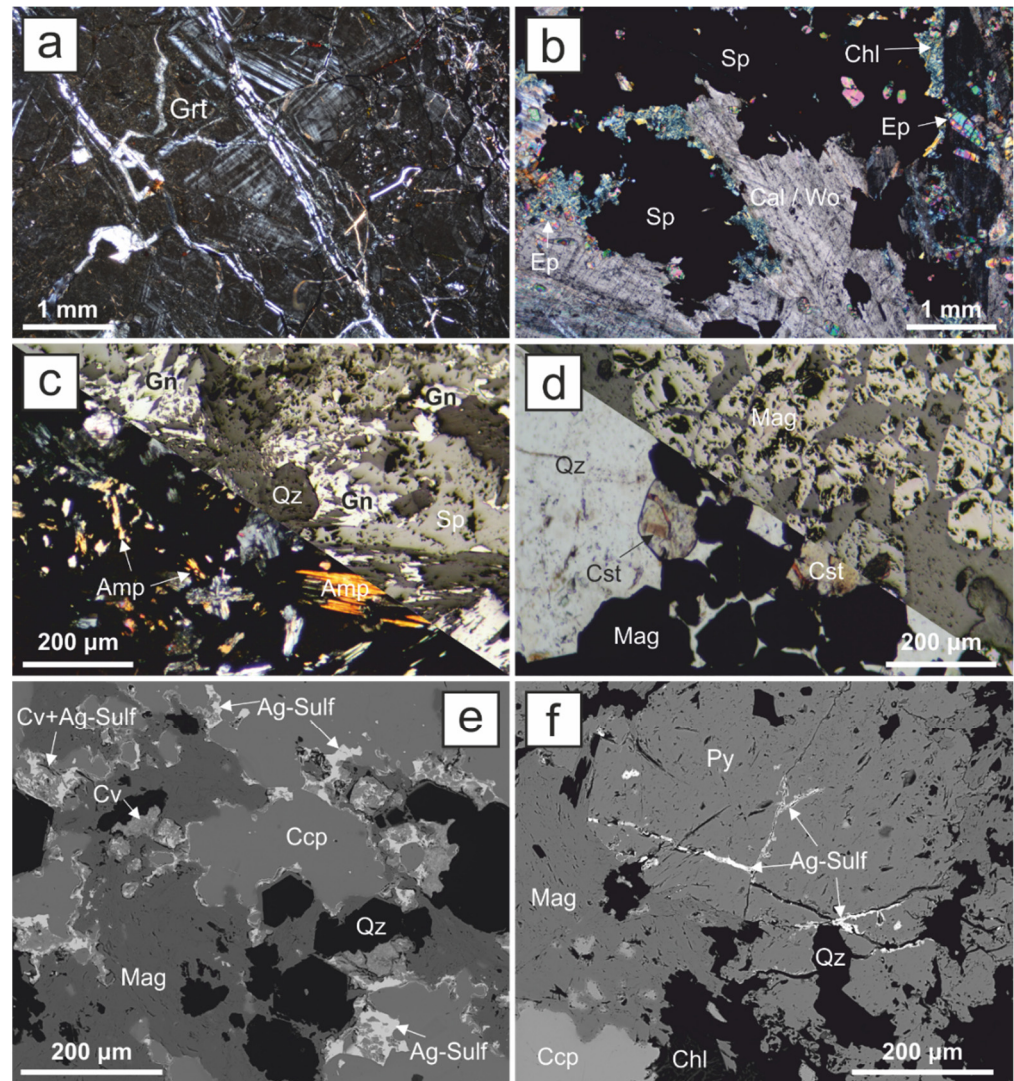


Figure 7. Photomicrographs of the Barisonis orebody. The mineral assemblages include (a) garnets with birefringent rims; (b) epidote, chlorite and calcite pseudomorphs with interstitial sphalerite; (c) interstitial sulfides in the amphibole-quartz matrix; (d) magnetite with subordinate cassiterite in fluorite-quartz veins; (e) chalcopyrite-magnetite zones with thin rims of covellite and Ag-sulfides (acanthite-argentite); (f) Ag-sulfides and covellite veinlets cross-cutting pyrite. Grt = garnet; Amp = amphibole; Wo = wollastonite; Chl = chlorite; Ep = epidote; Qz = quartz; Cal = calcite; Mag = magnetite; Cst = cassiterite; Sp = sphalerite; Ccp = chalcopyrite; Gn = galena; Py = pyrite; Cv = covellite; Ag-Sulf = acanthite-argentite.

The ore minerals of Barisonis are magnetite, cassiterite, bismuthinite, sphalerite, chalcopyrite, bornite, tetrahedrite, pyrite, galena, covellite and argentite-acanthite. Magnetite occurs in parallel seams of sub-millimetric euhedral-to-subhedral crystals in a quartz-fluorite and chlorite assemblage. Moreover, these crystals are often enveloping smaller hematite grains and have a skeletal structure. Hematite and goethite are also commonly found within fractures of garnets. Idiomorphic cassiterite crystals, up to 200 µm in size,

have also been found leaning on the edges of magnetite (Figure 7d). The formation of sulfides clearly postdates the retrograde stage as suggested by their recurrence in the intergranular spaces in chlorite-epidote-calcite and amphiboles aggregates (Figure 7b,c). Where retrograde alteration is not developed, sulfides are deposited in the intergranular spaces between prograde calcsilicates. Based on the abundance of inclusions and Fe contents, two sphalerite types can be distinguished. The first type is characterized by abundant chalcopyrite and pyrrhotite inclusions, a darker color and higher Fe contents (4–7 wt.%). The chalcopyrite-pyrrhotite inclusions are usually smaller along the edges of sphalerite crystals and become larger and more randomly distributed at the core. Conversely, the absence of inclusions, the brownish-red colors and the negligible Fe contents are characteristics of sphalerites of the second type. Chalcopyrite forms abundant anhedral grains and veinlets usually adjacent to sphalerite in the chlorite-titanite matrix and cross-cutting veinlets in garnet. Galena and pyrite are also interstitial to the retrograde skarn assemblage and surrounded by the previous sulfides. In addition, small grains of secondary Cu-sulfides such as bornite, chalcocite and thin veinlets of covellite formed at the expense of chalcopyrite. Secondary Ag-sulfides, which may be attributed to argentite or acanthite (Ag₂S), have been identified in several micrometer-sized anhedral crystallites both disseminated within the Zn-Cu-Pb-Fe sulfides and in the covellite veinlets cross-cutting pyrite and chalcopyrite (Figure 7e,f). Moreover, native-Au particles smaller than 10 µm have also been occasionally detected in the quartz matrix. The formation of goethite and cuprite rims on magnetite-pyrite and chalcopyrite, respectively, is related to a supergene stage.

6.2. Mitza Sermentus

Five samples from the Mitza Sermentus locality have been studied with the aim of highlighting the main differences between skarns formed on the limestone slices (MS.01; MS.02b; MS.3b; MS.04) and on mafic dykes (MS.3a). The formers are mainly characterized by clinopyroxene and wollastonite as the prevalent prograde minerals; garnets have been occasionally identified as isolated and strongly altered crystals, therefore with a certain degree of uncertainty. The most recurrent assemblage is characterized by bands of chlorite and calcite pseudomorphs after wollastonite (Figure 8b). These minerals often envelop fragmented individuals and aggregates of clinopyroxenes, epidotes and the relict garnets. Amphiboles and epidotes are usually more abundant where clinopyroxene alteration is more advanced. Occasionally, apatite and plagioclase have also been identified as accessory minerals. The ore minerals are sphalerite, chalcopyrite, pyrrhotite, pyrite and galena. Sphalerite occurs as interstitial grains characterized by moderately abundant chalcopyrite and pyrrhotite inclusions, usually randomly distributed. Occasionally, in the same way as the Fe-rich generation of the Barisonis samples, these inclusions are finer at the boundaries and larger at the core of sphalerite crystals. Chalcopyrite forms as void-filling grains in the matrix often associated with sphalerite. In the latter case, chalcopyrite corrodes and substitutes sphalerite as suggested by reaction gulfs at their boundaries. Subsequently, pyrite and galena are formed. Accessory minerals are tetrahedrite and bornite, usually observed at the edges of chalcopyrite. Calcite and quartz are the latest to form.

The sample MS.3a represents the contact between a skarn vein and the dark shale wall-rock in which the mineralized vein is enclosed (Figure 8a), adjacent to a metasomatized mafic dike (MS.3b). The shale matrix mainly consists of muscovite, chamosite and interstitial quartz arranged along a mylonitic foliation with folds and crenulation bands. Accessory minerals are represented by K-feldspar, plagioclase, clinozoisite, titanite and calcite. The mineralized zone is a centimeter-wide vein parallel to the main foliation. The contact with the skarn vein is marked by a band of a Ba-rich silicate phase in large (up to 3 mm) anhedral to subhedral crystals (Figure 8c,e). The EDS spectra point towards armenite, a rare silicate with the $\text{BaCa}_2\text{Al}_6\text{Si}_9\text{O}_{30} \cdot 2(\text{H}_2\text{O})$ formula, which is believed to form after hydrothermal alteration of baryte or Ba-rich feldspars; the armenite occurrence has been conclusively confirmed by XRPD analyses on the veinlets [59]. Occasional smaller armenite crystals also occur in the phyllite. The mineral assemblage is made of clinopyrox-

ene, amphibole, epidote, chlorite and wollastonite, the latter occasionally overgrown by pseudomorphic calcite. Accessory minerals are titanite, apatite, pumpellyite, armenite and barite (Figure 8c).

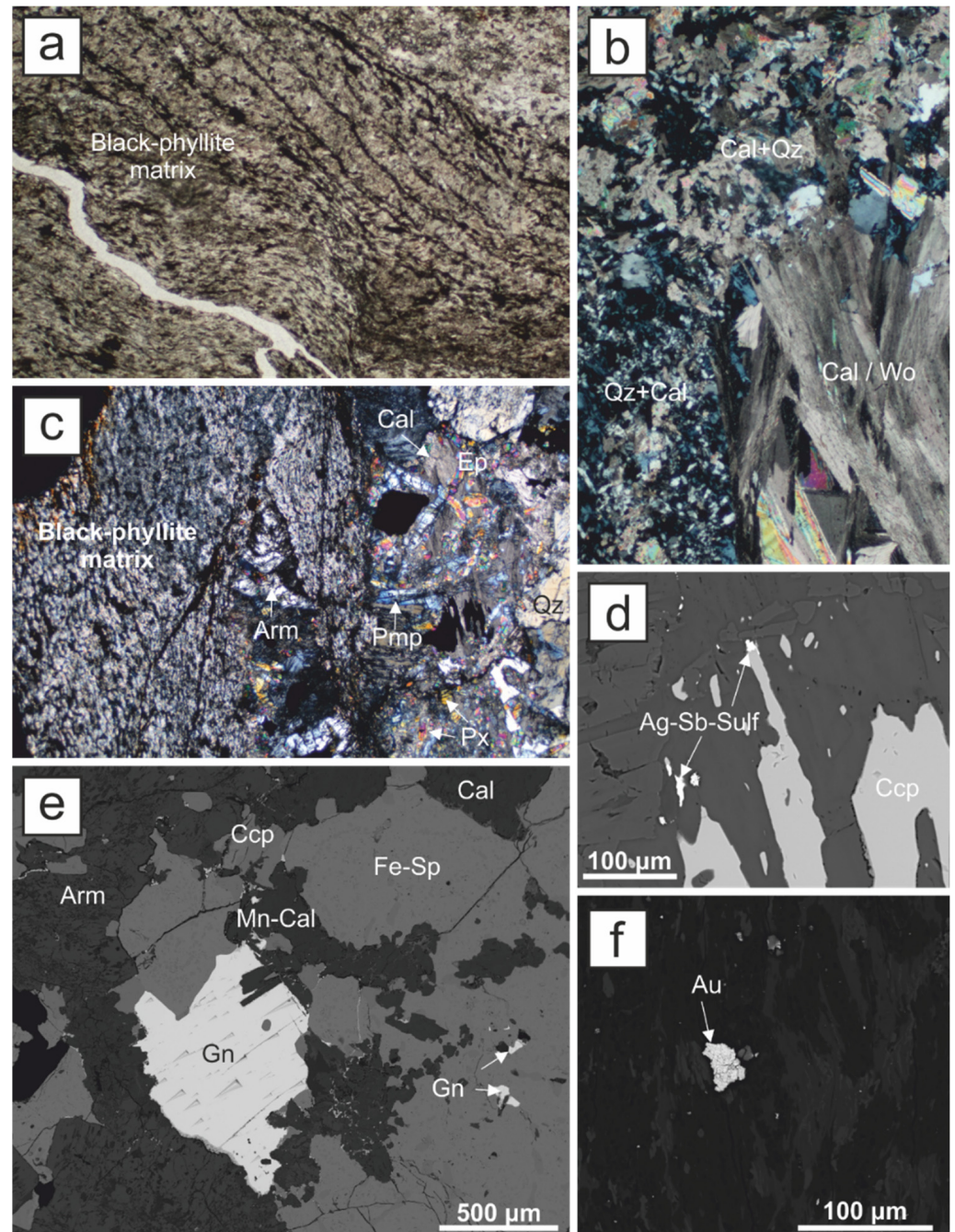


Figure 8. (a) Photomicrographs of the Mitza Sermentus orebody in the proximity of the black-phyllite host rock. Black domains are the mylonitic foliation. Mineral assemblages include (b) calcite-quartz replacing wollastonite; (c) chalcopyrite veinlets in a pyroxene-epidote-quartz-calcite gangue with subordinate pumpellyite, armenite, titanite and apatite; (d) Ag-sulfantimonides (tetrahedrite) grains associated with chalcopyrite; (e) galena, chalcopyrite and sphalerite in the armenite-rich zones; (f) native Au grains in the titanite, armenite, chlorite, epidote matrix. Mn-Cal = manganocalcite; Arm = armenite; Pmp = pumpellyite; Fe-Sp = Fe-rich sphalerite; Ag-Sb-Sulf = Ag-sulfantimonides (tetrahedrite); Au = native gold.

Similar to the BS samples, the ore minerals mainly consist of galena, sphalerite, chalcopyrite and pyrite. The first minerals to form in the crystallization sequence of sulfides are sphalerite and chalcopyrite, followed by galena and late pyrite. Chalcopyrite is also found in sparse inclusions within sphalerite, suggesting their partial timing overlap or the presence of two generations of chalcopyrite. Moreover, and similar to the BS samples, Ag-sulfosalts and Au have also been found (Figure 8d,f). Here, though, the former are more abundant and host a significant amount of antimony (up to 11 wt.% of Sb), therefore suggesting their occurrence in the form of tetrahedrite over Ag-sulfides. Small particles (up to 20 μm) of native Au have been recognized in the titanite, armenite, chlorite, epidote matrix (Figure 8f). Later veins of quartz, calcite and manganocalcite intrude both the phyllite and the mineralized vein.

6.3. S'Ega Su Forru

Due to the limited size of the S'Ega Su Forru mineralized vein, one sample (namely FOR1) was chosen as representative of this orebody. It consists of a matrix made up by calc-silicate minerals as prograde clinopyroxene of the diopside-hedenbergite series slightly enriched in Mn (up to 2.5 wt%), partially replaced by amphibole, epidote and chlorite. The ore minerals mainly consist of base metal sulfides as sphalerite, pyrite, chalcopyrite and galena. A peculiar feature of this mineralization, not found in the other outcrops within the Rosas mine area, is the presence of Ni-Co-Fe sulfarsenides (Figure 9a–c). Indeed, SEM-EDS analyses revealed the presence of small (5–15 μm) subrounded and idiomorphic grains of Co-Ni-Fe sulfarsenides, sometimes isolated, some others grouped in small clusters, disseminated around the calcsilicate matrix and as tiny inclusions in pyrite. The composition of these phases is characterized by almost constant contents of As (40–42 wt.%) and S (20–22 wt.%) indicating a As:S = 1:1 molar ratio (mono-sulfarsenides). Conversely, the contents of Co, Ni and Fe are strongly variable from one point to another, with Co ranging between 16 and 29 wt.%, Ni 3–11 wt.% and Fe 4–8 wt.%. Co is inversely related to both Ni and Fe, whereas a clear correlation between Ni and Fe is not observed. In addition, traces of Zn and Cu are locally found. The As/S constant ratio and the continuous variation of Co, Ni and Fe point towards a mixture of glaucodot ((Co,Fe)AsS) and gersdorffite (NiAsS). Pyrite also forms idiomorphic cubic crystals up to 0.4 mm locally with Ni-Co-Fe arsenides and sphalerite inclusions. Chalcopyrite can be found as anhedral grains at contact with pyrite. Inclusions are rare and consist mostly of micro-scale individuals of sphalerite and pyrite. Sphalerite forms large anhedral grains cross-cutting chalcopyrite. Its dark color is due to Fe contents up to 10%; traces of Mn have also been detected; “chalcopyrite disease” [61] textures are very frequent. The size of the chalcopyrite inclusions increases towards the center portion of sphalerite grains where pyrite inclusions have also been recurrently observed. Galena grains fill the intergranular spaces between previous sulfides, often producing fractures on sphalerite and chalcopyrite (Figure 9b,c). Small aggregates of hematite lamellae form at the expense of pyrite crystals and represent the late stage of the ore minerals formation.

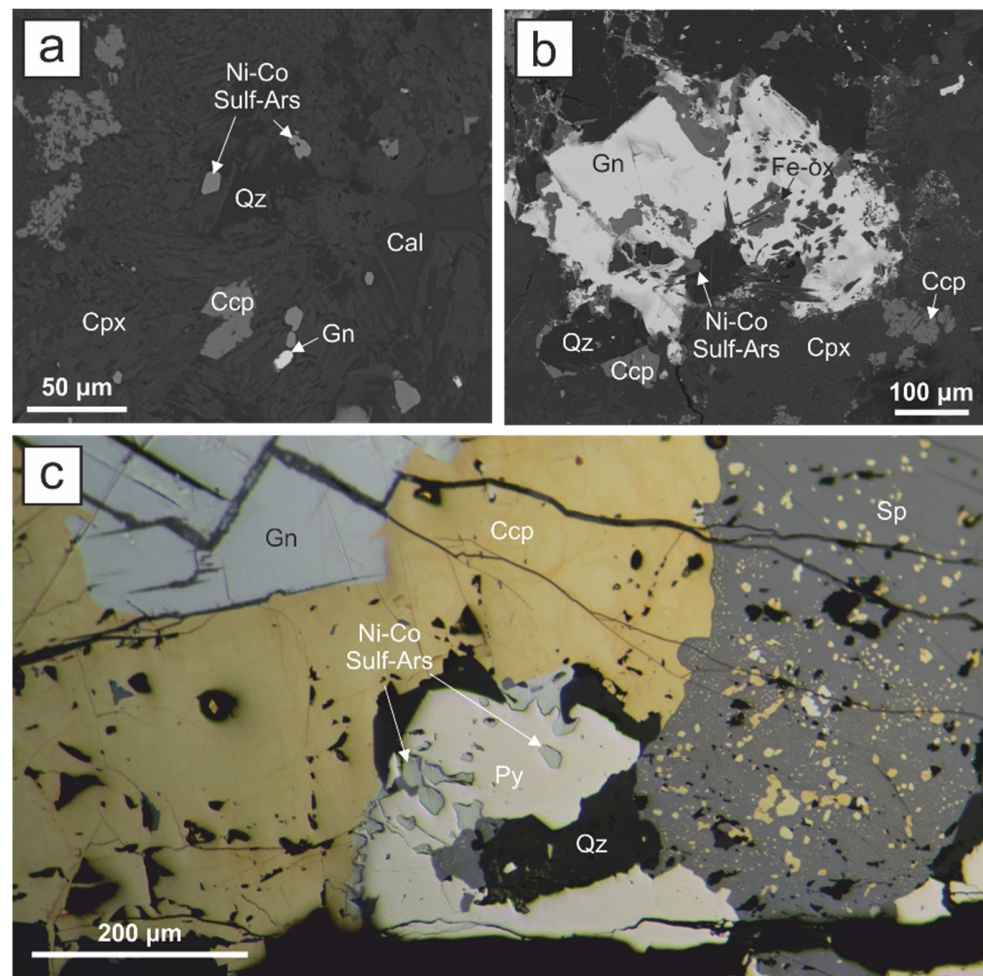


Figure 9. Photomicrographs of the S'Ega Su Forru vein: (a) a clinopyroxene-quartz-calcite matrix with base metal sulfides and Ni-Co-Fe sulfarsenides; (b) galena and Fe-oxides (goethite-hematite) enveloping Ni-Co sulfarsenide crystals; (c) Ni-Co sulfarsenides enclosed in pyrite with sphalerite, chalcopyrite and galena. Cpx = clinopyroxene; Ni-Co-Sulf-Ars = Ni-Co sulfarsenides; Fe-Ox = Fe-oxides (goethite-hematite).

7. Discussion

In the following, we discuss how the deformation events led to the structural setting that favored the fluid circulation and mineralization in the RSZ and how localized contact metamorphism and widespread metasomatic processes gave rise to the peculiar paragenesis of skarn ores in the Rosas mining district.

The tectonic slices of limestones embedded within a highly sheared siliciclastic succession are the main structural feature of the study area, and they constitute widespread discontinuities that had allowed the fluid circulation and the skarn ore mineralization. The structuring of the plumbing system of the RSZ reflects a progressive deformation occurred in a compressive setting that led, in sequence, to the development of recumbent folds and related axial plane cleavage, thrusts development and bedding transposition along the tectonic foliation. It is in this context that the tectonic slices took place, most probably by means of thrusts that enucleated shearing the stratigraphic contacts in the overturned limbs of the recumbent folds [62,63], separating large portions of limestones and translating them within the siliciclastic succession. Note that the limestones are lower Cambrian in age, and the siliciclastic succession is upper Ordovician in age, and no evidence of older siliciclastic formations occurs in the RSZ, except for a small slice of Cabitza Fm. This suggests a remarkable displacement and/or a scarce thickness of the Cabitza Fm. above the limestones,

likely because of the erosion related to the Sardinian Phase [33,38]. The thrusts envelop the limestone slices with an anastomosed geometry and played the role of preferential conduits for fluids because they are zone of weakness with higher permeability than the surrounding rocks [64,65].

The compressive regime is followed by extension processes due to the chain's collapse that led to the exhumation of the RSZ to shallower structural levels; during this stage, folds with horizontal axial plane developed, affecting mainly the weaker siliciclastic succession and its cleavage. The decreasing of the lithostatic stress as exhumation progresses, as well as the weakness induced by the penetrative cleavage, favored the intrusion of mafic dykes that postdate the compressive phases, as testified by the fact that the dyke is not foliated. The attitude of the mafic dykes is parallel to the general setting of the RSZ, suggesting that their intrusion exploited this large discontinuity. Locally, however, the dykes cut across the cleavage no more favorably oriented because they are affected by syn-exhumation folds, demonstrating that the mafic dyke intrusion postdate also the exhumation phases.

Thus, the network of thrusts and the increased permeability provided by the pervasive foliation allowed the fluids to rise from deeper levels and to reach the limestones. The tectonic slices acted as a trap for the mineralizing fluids, due to the higher reactive potential of the carbonate rocks [15].

Metamorphic and metasomatic processes selectively affected the carbonate tectonic slices, originating several skarn-type orebodies. In general, mineralized rocks display the mineralogical assemblages and textures of Fe-Cu-Zn skarns, with relics of anhydrous calcic phases related to the prograde metamorphic stage (andradite/grossular anisotropic garnet, clinopyroxene, wollastonite), frequently enclosed in a mass of hydrated phases (actinolitic amphibole, epidote) and magnetite related to the retrograde metasomatic stage, in turn followed by chlorite, sulfides, quartz and calcite associated to the hydrothermal stage. Sulfide ores predominantly consist of sphalerite, chalcopyrite and galena, with abundant pyrite and pyrrhotite and minor tetrahedrite and Ag-sulfosalts.

The style of the skarn mineralization in the three studied examples, namely Barisonis, Mitza Sermentus and S'Ega Su Forru, slightly varies according to the local structural framework where the orebodies are emplaced: small limestones slices adjacent to the mafic dyke (Barisonis); small limestones slices embedded in a highly sheared siliciclastic succession (Mitza Sermentus); a discrete thrust fault at the bottom of larger limestone slice (S'Ega Su Forru). In the following, these differences are discussed.

In the Barisonis mineworking, the skarn developed in a carbonate slice directly in contact with the mafic dyke and is characterized by a clear and well-developed zoning pattern. Considering that such a stratigraphic relationship and zonation have not been observed in other skarns of the RSZ, we can speculate a correlation between the potential contact metamorphism induced by the mafic dyke emplacement and the zoning pattern. In particular, contact metamorphism effects might have given rise, at the gabbro-carbonate tectonic slices contacts, to the metric to decametric garnet, pyroxene and wollastonite mineralogical zonation recognized in the Barisonis mineworking. Retrograde and ore-bearing hydrothermal stages display mineral associations and textures that suggest a common origin with the other studied mineralization in the area.

The style of mineralization in Mitza Sermentus area is characterized by several metasomatized carbonate lenses, metasomatized mafic dikes and thin mineralized veinlets parallel to the tectonic foliation. This area is structurally located close to the thrust that emplaced the Monte Argentu Fm. above the Monte Orri Fm. This shear zone is not as discrete as the thrusts that bound the carbonate tectonic slices, most probably because it developed at the contact with weak siliciclastic formations and the shortening has been accommodated in a wide zone where the mylonitic foliation acted as an active foliation [25]. This allowed the mineralizing fluids to precipitate extensively within the foliation planes, originating a peculiar mineralization style where no evidence of metamorphic zonation can be found. This style of mineralization could be confused with a stratabound type, misinterpreting

the tectonic foliation as a bedding, or as a stockwork type, nor recognizing the structural control and so leading to a wrong prospection of the orebody.

The orebody in S'Ega Su Forru mine is smaller than those of Barisonis and Mitza Sermentus and consists of a 20 cm thick vein located at the tectonic contact between the carbonate slice and the siliciclastic succession of the Monte Orri Fm. In this case, the structural control of the mineralization is strictly related to the fault damage zone of the bottom thrust of the slices, where the flow of the mineralized fluid is enhanced by the higher permeability.

The field surveys and the observations above about the three different styles of mineralization pointed out the tight structural controls on skarn and ore localization and distribution.

The structural and mineralogical data suggest that the structural evolution and its control on the ore mineralization distribution evolved in three stages (Figure 10): (1) the first stage is the structuring of the plumbing system of the RSZ as a consequence of the collisional phases related to the Variscan Orogeny. The pressure solution and grain boundary sliding deformation mechanisms that accommodated the strain in the RSZ suggest P-T conditions in the range of 3–3.5 kbar, thus we can consider a depth of about 11.5–13.5 km, and a temperature of 250–300 °C [16]. (2) The second stage concerns the intrusion of the mafic dyke and its related swarm of small veinlets. In particular, the 100-m-thick mafic dyke induced a contact metamorphism aureole whose zonation is recognizable only in some of the skarns. The intrusion of the mafic dyke occurred probably during the extensional phases related to the collapse of the Variscan chain that allowed the re-using of previous structures (foliation and thrust) as normal faults or extensional joint, at very shallow crustal structural levels. (3) The third stage reflects a larger scale, extensive magmatic fluid circulations that involved the structures of the RSZ and gave rise to the skarn ore mineralization. Infilling of metasomatic fluids in carbonate tectonic slices occurred along faults, also aided by metasomatic reactions and by the increase in permeability due to alteration of prograde stage minerals. Metasomatic reactions also involved mafic rocks, producing a mineral association of chlorite, epidote, plagioclase, K-feldspar and pumpellyite with accessory armenite, titanite and apatite. This mineral association allows us to ascribe the metamorphic and metasomatic processes to P-T conditions that do not exceed pressure of 2 kbar, so few kilometers in depth, and a temperature range of roughly 200–350 °C [66,67].

The causative intrusions related to skarn ores belong to the GS1 suite [17] of early Permian (289 Ma) ilmenite-series, ferroan granites which intrude the RSZ about 3 km east from the studied area, beneath which the granites are most probably present as well. The geochemical signatures and mineralogical associations of the skarn ores (e.g., presence of fluorite and cassiterite) are significant elements in favor of the metallogenic relationship with the GS1 granites. The Fe-Cu-Zn skarn ores of Rosas are best interpreted as distal orebodies whose localization is controlled by inherited structures, connected to large-scale circulation of granite-related fluids in the km-sized plumbing system represented by the RSZ.

The emplacement of the skarns of the RSZ mine district is an example of a passive structural control of ore mineralization localization. The main evidences are (1) the orebodies aligned with the main structural features, thrusts and tectonic foliation, both at cartographic and outcrop scale; (2) the orebodies show no deformation neither evidence of preferential orientation at thin section scale; (3) the plumbing system has been structured at crustal structural levels definitely deeper than that where the formation of the skarn occurred, which is very shallow and in a completely different tectonic scenario.

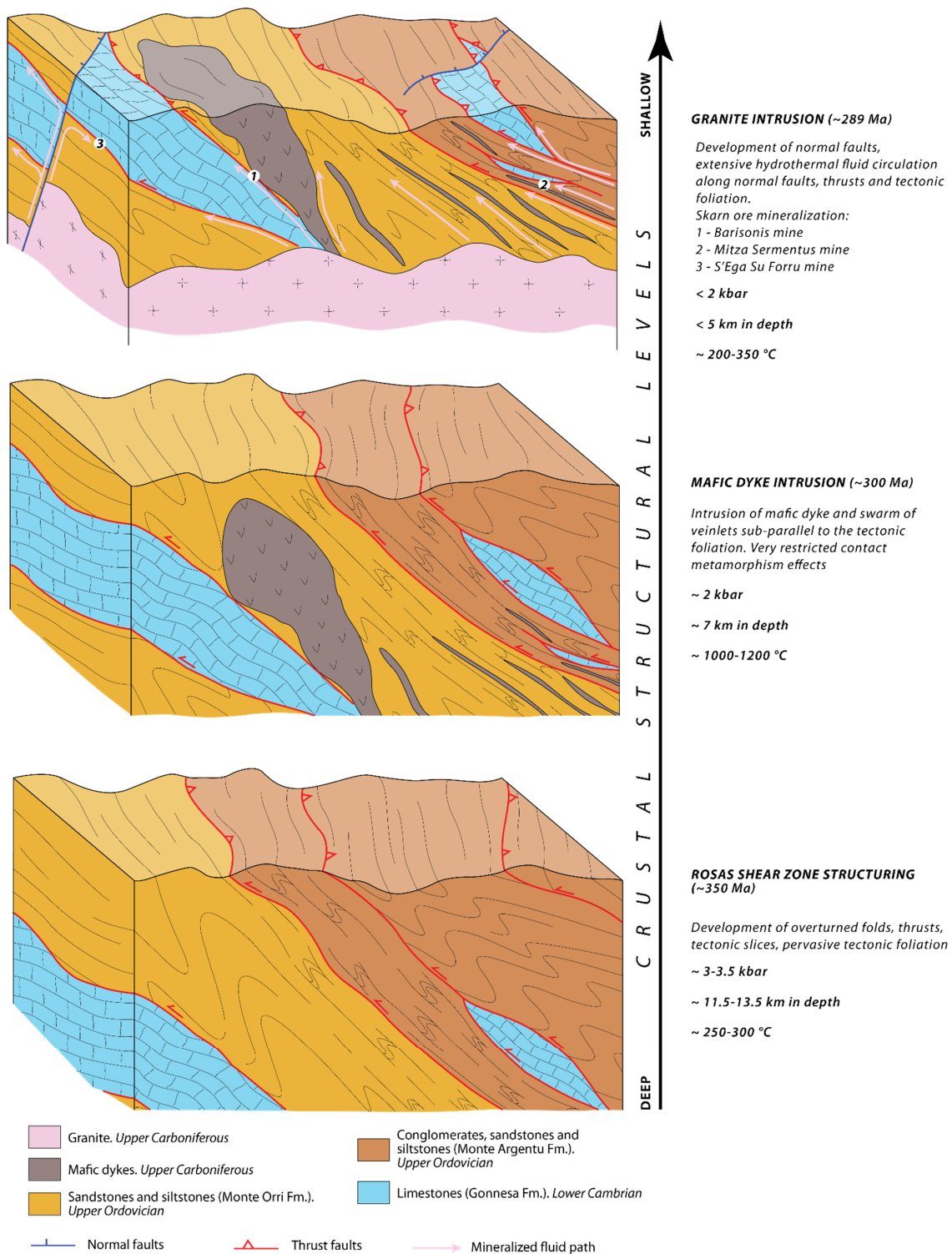


Figure 10. Cartoon showing the tectonic evolution and the passive structural control on the skarn ore mineralization in the Barisonis (1), Mitza Sermentus (2) and S'Ega Su Forru (3) mines. The plumbing system is inherited from the structuring of the Rosas Shear Zone at deep structural levels. Once exhumed at shallow structural levels, the Rosas Shear Zone acted as weakness and permeable zone favorable for the intrusion of mafic dyke and, soon after, for extensive granite-related fluid circulation. The ages of each step are supposed taking into account the available dating in the Sardinian basement of the regional metamorphism (~350 Ma, [68]), mafic dyke intrusion (~300 Ma, [41,69,70]) and granite intrusion (~289 Ma [17,42]).

8. Conclusions

The field survey and structural analysis in the RSZ and ore microscopy and SEM-EDS analysis allowed us to better characterize the skarn deposits in the Rosas mining district, excluding any sedimentary process involved in the genesis of the ores as proposed up to now.

The skarn ores in the RSZ mining district are an example of passive structurally controlled mineralization localization in polydeformed basements. The structuring of the RSZ during the collisional phases of the Variscan Orogeny originated at the brittle–ductile transition crustal level and acted as the plumbing system exploited, at shallower crustal levels, during the extensional phases related to the collapse of the Variscan chain, by the mafic dyke intrusion and by extensive magmatic fluid circulation related to the granite emplacement. In addition to the different crustal levels of the plumbing system structuring and ores emplacement, the passive structural control on the mineralization location and distribution is testified by the same attitude between the orebodies and the structures and by the lack of deformation in the mafic dyke and skarn. The paragenesis of the ores and the mineralization style varies slightly according to the local structural setting where skarns took place: a carbonate tectonic slice adjacent to the mafic dyke; an intensely sheared zone; a discrete thrust fault surface.

The intrusion of the mafic dyke generated a local-scale contact metamorphic aureole on the limestone slices (for instance in the Barisonis skarn) that, once affected by the subsequent metasomatic processes, gave rise to a well recognizable zonation pattern in the skarn ores and to the occurrence of peculiar minerals in the mafic protolith. The limited extent of thermal metamorphism induced by mafic dykes, despite their likely high temperature, can be explained by the quick cooling of these relatively small bodies.

Finally, the results suggest that the understanding of the structural style and its control in the ore mineralization localization is essential for a proper identification, quantification and exploitation of economically relevant ore minerals, especially in complex structural settings of polydeformed basements.

Author Contributions: Conceptualization, S.N., A.F., A.A., F.C., M.L.D. and D.F.; methodology, A.A., M.L.D., D.F., S.N., F.C. and A.F.; microscope analysis, A.A., M.L.D., D.F. and S.N.; field investigation, A.A., A.F., S.N., M.L.D. and F.C.; data curation, F.C., A.A., M.L.D., D.F., A.F. and S.N.; writing—original draft preparation, F.C., A.A., M.L.D., D.F. and S.N.; writing—review and editing, S.N. and A.F.; supervision, S.N. and A.F.; funding acquisition, A.F. and S.N. All authors have read and agreed to the published version of the manuscript.

Funding: This work was supported by Fondazione di Sardegna (research program: “Sustainable land management: the tools of geology for the environment”—CUP F75F21001270007), and Regione Autonoma della Sardegna (research program: “Il blocco Sardo-Corso: area chiave per la ricostruzione della geodinamica varisica”—CUP J81G17000110002). Matteo Luca Deidda gratefully acknowledges Sardinia Regional Government for the financial support of his PhD scholarship (P.O.R. Sardegna F.S.E. Operational Programme of the Autonomous Region of Sardinia, European Social Fund 2007–2013—Axis IV Human Resources, Objective 1.3, Line of Activity 1.3.1.).

Data Availability Statement: Not applicable.

Acknowledgments: We thank two anonymous reviewers for their careful comments and suggestions that improved the quality of the paper. We acknowledge the CeSAR (Centro Servizi d’Ateneo per la Ricerca) of the University of Cagliari, Italy, for SEM analysis.

Conflicts of Interest: The authors declare no conflict of interest.

References

1. Cox, S.F.; Knackstedt, M.A.; Braun, J. Principles of structural control on permeability and fluid flow in hydrothermal systems. In *Structural Controls on Ore Genesis*; Richards, J.P., Tosdal, R.M., Eds.; Reviews in Economic Geology; Society of Economic Geologists: Littleton, CO, USA, 2001; Volume 14, pp. 1–24.
2. Cathles, L.M. Fluid flow and genesis of hydrothermal ore deposits. In *Economic Geology 75th Anniversary Volume, 1905–1980*; Society of Economic Geologists: Littleton, CO, USA, 1981; pp. 424–457. [[CrossRef](#)]

3. Caine, J.S.; Evans, J.P.; Forster, C.B. Fault zone architecture and permeability structure. *Geology* **1996**, *24*, 1025–1028. [[CrossRef](#)]
4. Ingebritsen, S.E.; Appold, M.S. The physical hydrogeology of ore deposits. *Econ. Geol.* **2012**, *107*, 559–584. [[CrossRef](#)]
5. Ord, A.; Lester, D.R.; Hobbs, B.E. The mechanics of hydrothermal systems: I. Ore systems as chemical reactors. *Ore Geol. Rev.* **2012**, *49*, 1–44. [[CrossRef](#)]
6. Lester, D.R.; Ord, A.; Hobbs, B.E. The mechanics of hydrothermal systems: II. Fluid mixing and chemical reactions. *Ore Geol. Rev.* **2012**, *49*, 45–71. [[CrossRef](#)]
7. Chauvet, A. Structural Control of Ore Deposits: The Role of Pre-Existing Structures on the Formation of Mineralised Vein Systems. *Minerals* **2019**, *9*, 56. [[CrossRef](#)]
8. Funedda, A.; Naitza, S.; Butta, C.; Cocco, F.; Dini, A. Structural Controls of Ore Mineralization in a Polydeformed Basement: Field Examples from the Variscan Bacca Locci Shear Zone (SE Sardinia, Italy). *Minerals* **2018**, *8*, 456. [[CrossRef](#)]
9. Sibson, R.H. Earthquake rupturing as a mineralizing agent in hydrothermal systems. *Geology* **1987**, *15*, 701–704. [[CrossRef](#)]
10. Sibson, R.H. Fault-valve behavior and the hydrostatic lithostatic fluid pressure interface. *Earth Sci. Rev.* **1992**, *32*, 141–144. [[CrossRef](#)]
11. Hodgson, C.J. The structure of shear-related, vein-type gold deposits: A review. *Ore Geol. Rev.* **1989**, *4*, 231–273. [[CrossRef](#)]
12. Stephens, J.R.; Mair, J.R.; Oliver, N.H.L.; Hart, C.J.R.; Baker, T. Structural and mechanical controls on intrusion-related deposits of the Tombstone Gold Belt, Yukon, Canada, with comparisons to other vein-hosted ore-deposit types. *J. Struct. Geol.* **2004**, *26*, 1025–1041. [[CrossRef](#)]
13. Cox, S.F. Coupling between Deformation, Fluid Pressures, and Fluid Flow in Ore-Producing Hydrothermal Systems at Depth in the Crust. In *Economic Geology 100th Anniversary Volume, 1905–2005*; Society of Economic Geologists: Littleton, CO, USA, 2005; pp. 39–75. [[CrossRef](#)]
14. Cox, S.F. Injection-Driven Swarm Seismicity and Permeability Enhancement: Implications for the Dynamics of Hydrothermal Ore Systems in High Fluid-Flux, Overpressured Faulting Regimes—An Invited Paper. *Econ. Geol.* **2016**, *111*, 559–587. [[CrossRef](#)]
15. Meinert, L.D.; Dipple, G.M.; Nicolescu, S. World Skarn Deposits. In *Economic Geology 100th Anniversary Volume, 1905–2005*; Society of Economic Geologists: Littleton, CO, USA, 2005; pp. 299–336. [[CrossRef](#)]
16. Casini, L.; Funedda, A.; Oggiano, G. A balanced foreland–hinterland deformation model for the Southern Variscan belt of Sardinia, Italy. *Geol. J.* **2010**, *45*, 634–649. [[CrossRef](#)]
17. Conte, A.M.; Cuccuru, S.; D’Antonio, M.; Naitza, S.; Oggiano, G.; Secchi, F.; Casini, L.; Cifelli, F. The post-collisional late Variscan ferroan granites of southern Sardinia (Italy): Inferences for inhomogeneity of lower crust. *Lithos* **2017**, *294–295*, 263–282. [[CrossRef](#)]
18. Carmignani, L.; Carosi, R.; Di Pisa, A.; Gattiglio, M.; Musumeci, G.; Oggiano, G.; Pertusati, P.C. The Hercynian chain in Sardinia (Italy). *Geodin. Acta* **1994**, *7*, 31–47. [[CrossRef](#)]
19. Franceschelli, M.; Puxeddu, M.; Cruciani, G. Variscan metamorphism in Sardinia, Italy: Review and discussion. *J. Virtual Explor.* **2005**, *19*, 1–36. [[CrossRef](#)]
20. Conti, P.; Patta, E.D. Large-scale Hercynian West-directed tectonics in southeastern Sardinia (Italy). *Geodin. Acta* **1998**, *11*, 217–231. [[CrossRef](#)]
21. Conti, P.; Carmignani, L.; Funedda, A. Change of nappe transport during the Variscan collisional evolution of central-southern Sardinia (Italy). *Tectonophysics* **2001**, *332*, 255–273. [[CrossRef](#)]
22. Conti, P.; Carmignani, L.; Oggiano, G.; Funedda, A.; Eltrudis, A. From thickening to extension in the Variscan belt-kinematic evidence from Sardinia (Italy). *Terra Nova* **1999**, *11*, 93–99. [[CrossRef](#)]
23. Rossi, P.; Cocherie, A. Genesis of a Variscan batholith: Field, petrological and mineralogical evidence from the Corsica-Sardinia batholith. *Tectonophysics* **1991**, *195*, 319–346. [[CrossRef](#)]
24. Casini, L.; Cuccuru, S.; Puccini, A.; Oggiano, G.; Rossi, P. Evolution of the Corsica–Sardinia Batholith and late-orogenic shearing of the Variscides. *Tectonophysics* **2015**, *646*, 65–78. [[CrossRef](#)]
25. Funedda, A. Foreland- and hinterland-verging structures in fold-and-thrust belt: An example from the Variscan foreland of Sardinia. *Int. J. Earth Sci.* **2009**, *98*, 1625–1642. [[CrossRef](#)]
26. Carmignani, L.; Oggiano, G.; Funedda, A.; Conti, P.; Pasci, S. The geological map of Sardinia (Italy) at 1:250,000 scale. *J. Maps* **2016**, *12*, 826–835. [[CrossRef](#)]
27. Teichmüller, R. Zur Geologie der Thyrrenisgebietes. Teil 1: Alte und junge Krunstenbewegungen im südlichen Sardinien. *Ges. Der Wiss. Zu Göttingen* **1931**, *3*, 857–950.
28. Stille, H. Bemerkungen betreffend die “sardische Faltung” und den Ausdruck “ophiolitisch”. *Z. Geol. Ges.* **1939**, *91*, 771–773.
29. Von Raumer, J.F.; Stampfli, G.M.; Arenas, R.; Sánchez Martínez, S. Ediacaran to Cambrian oceanic rocks of the Gondwana margin and their tectonic interpretation. *Int. J. Earth Sci.* **2015**, *104*, 1107–1121. [[CrossRef](#)]
30. Cocco, F.; Oggiano, G.; Funedda, A.; Loi, A.; Casini, L. Stratigraphic, magmatic and structural features of Ordovician tectonics in Sardinia (Italy): A review. *J. Iber. Geol.* **2018**, *44*, 619–639. [[CrossRef](#)]
31. Cocco, F.; Funedda, A. The Sardinic Phase: Field evidence of Ordovician tectonics in SE Sardinia, Italy. *Geol. Mag.* **2019**, *156*, 25–38. [[CrossRef](#)]
32. Oriolo, S.; Schulz, B.; Geuna, S.; González, P.D.; Otamendi, J.E.; Sláma, J.; Druguet, E.; Siegesmund, S. Early Paleozoic accretionary orogens along the Western Gondwana margin. *Geosci. Front.* **2021**, *12*, 109–130. [[CrossRef](#)]
33. Pillola, G.L.; Leone, F.; Loi, A. The Cambrian and Early Ordovician of SW Sardinia. *G. Di Geol.* **1998**, *60*, 25–38.

34. Bechstädt, T.; Boni, M. *Sedimentological, Stratigraphical and ore Deposits Field Guide of the Autochthonous Cambro-Ordovician of Southwestern Sardinia*; (Technical Periodicals) Descriptive Memories of the Geological Map of Italy; Istituto Superiore per la Protezione e la Ricerca Ambientale: Rome, Italy, 1994; Volume 48, 434p.
35. Elicki, O.; Pillola, G.L. Cambrian microfauna and palaeoecology of the Campo Pisano Formation at Gutturu Pala (Iglesiente, SW Sardinia, Italy). *Bollettino della Società Paleontologica Italiana* **2004**, *43*, 383–401.
36. Gandin, A. Depositional and paleogeographic evolution of the Cambrian in south-western Sardinia. In *Correlation of Prevariscan and Variscan Events of the Alpine-Mediterranean Mountain Belt*; IGCP Project No. 5—Newsletter; Sassi, F.P., Bourrouilh, R., Eds.; Institute of Mineralogy Petrology, University of Padua: Padua, Italy, 1989; Volume 7, pp. 151–166.
37. Laske, R.; Bechstädt, T.; Boni, M. The post-Sardic Ordovician series. In *Sedimentological, Stratigraphical and Ore Deposits Field Guide of the Autochthonous Cambro-Ordovician of Southwestern Sardinia*; Memorie Descrittive della Carta Geologica, d'Italia; Bechstädt, T., Boni, M., Eds.; Servizio Geologico d'Italia: Rome, Italy, 1944; pp. 115–146.
38. Leone, F.; Ferretti, A.; Hammann, W.; Loi, A.; Pillola, G.L.; Serpagli, E. A general view on the post-Sardic Ordovician sequence from SW Sardinia. *Rend. Soc. Paleontol. Ital.* **2002**, *1*, 51–68.
39. Gnoli, M.; Kříž, J.; Leone, F.; Olivieri, R.; Serpagli, E.; Storch, P. Lithostratigraphic units and biostratigraphy of the Silurian and early Devonian of Southwest Sardinia. *Boll. Della Soc. Paleontol. Ital.* **1990**, *29*, 11–23.
40. Barca, S.; Forci, A.; Forci, A. I depositi sinorogenici ercinici del Sulcis (Sardegna sud-occidentale). *Boll. Della Soc. Geol. Ital.* **1998**, *117*, 407–419.
41. Secchi, F.; Naitza, S.; Oggiano, G.; Cuccuru, S.; Puccini, A.; Conte, A.M.; Giovanardi, T.; Mazzucchelli, M. Geology of late-Variscan Sàrrabus pluton (south-eastern Sardinia, Italy). *J. Maps* **2021**, *17*, 591–606. [[CrossRef](#)]
42. Boni, M.; Stein, H.J.; Zimmerman, A.; Villa, I.M. Re-Os age for molybdenite from SW Sardinia (Italy): A comparison with $^{40}\text{Ar}/^{39}\text{Ar}$ dating of Variscan granitoids. In *Mineral Exploration and Sustainable Development*; Eliopoulos, D.G., Ed.; Millpress: Rotterdam, The Netherlands, 2003; pp. 247–250.
43. Naitza, S.; Oggiano, G.; Cuccuru, S.; Casini, L.; Puccini, A.; Secchi, F.; Funedda, A.; Tocco, S. Structural and magmatic controls on Late Variscan Metallogenesis: Evidences from Southern Sardinia (Italy). In Proceedings of the 13th Biennial SGA Meeting, Nancy, France, 24–27 August 2015; Volume 1, pp. 161–164.
44. Naitza, S.; Conte, A.M.; Cuccuru, S.; Oggiano, G.; Secchi, F.; Tecce, F. A Late Variscan tin province associated to the ilmenite-series granites of the Sardinian Batholith (Italy): The Sn and Mo mineralisation around the Monte Linas ferroan granite. *Ore Geol. Rev.* **2017**, *80*, 1259–1278. [[CrossRef](#)]
45. Carmignani, L.; Cocozza, T.; Ghezzi, P.C.; Pertusati, P.C.; Ricci, C.A. Outlines of the Hercynian Basement of Sardinia. In *Guide-book to the Excursion on the Paleozoic basement of Sardinia*; IGCP Project No. 5—Newsletter; Università di Siena: Siena, Italy, 1986; pp. 11–21.
46. Carosi, R.; Musumeci, G.; Pertusati, P.C.; Carmignani, L. The Hercynian backthrusts of eastern Iglesias (SW Sardinia): An example of inversion tectonics. In *Contributions to the Geology of Italy with Special Regard to the Paleozoic Basement*; IGCP No., 276—Newsletter; Carmignani, L., Sassi, F.P., Eds.; Università di Siena: Siena, Italy, 1992; pp. 97–105.
47. Cocco, F.; Funedda, A. Mechanical influence of inherited folds in thrust development: A case study from the Variscan fold-and-thrust belt in SW Sardinia (Italy). *Geosciences* **2021**, *11*, 276. [[CrossRef](#)]
48. Pasci, S.; Pertusati, P.C.; Salvadori, I.; Murtas, M. I rilevamenti CARG del foglio geologico 555 “Iglesias” e le nuove implicazioni strutturali sulla tettonica della “Fase Sarda”. *Rend. Online Della Soc. Geol. Ital.* **2008**, *3*, 614–615.
49. ISPRA. Carta Geologica d'Italia Alla Scala 1:50,000. Foglio 555 IGLESIAS. Available online: https://www.isprambiente.gov.it/Media/carg/555_IGLESIAS/Foglio.html (accessed on 16 January 2022).
50. Boni, M.; Balassone, G.; Iannace, A. Base metal ores in the lower Paleozoic of southwestern Sardinia. *Soc. Econ. Geol. Spec. Publ.* **1996**, *4*, 18–28. [[CrossRef](#)]
51. Valera, R.; Zuffardi, P. Segnalazione di Scheelite in taluni adunamenti metamorfici della Sardegna (Nota preliminare). *Res. Ass. Min. Sarda* **1968**, *73*, 62–64.
52. Valera, R.; Zuffardi, P. La geochimica del tungsteno nel Paleozoico della Sardegna. *Rend. Soc. Ital. Mineral. Petrol.* **1970**, *26*, 815–830.
53. Pirri, I.V. Il giacimento a blenda, galena, calcopirite di Sa Marchesa nel Sulcis (Sardegna). *Boll. Soc. Ital. Sci. Nat.* **1971**, *62*, 505–549.
54. Funedda, A.; Carmignani, L.; Pasci, S.; Patta, E.D.; Uras, V.; Conti, P.; Sale, V. Foglio 556 ASSEMINI. In *Note Illustrative della Carta Geologica d'Italia alla Scala 1:50,000, Servizio Geologico d'Italia*; Istituto Poligrafico e Zecca dello Stato: Roma, Italy, 2009; p. 192.
55. Valera, R. Appunti sulla morfologia, termometria e composizione delle inclusioni fluide di fluoriti sarde. *Rend. Soc. Ital. Mineral. Petrol.* **1974**, *30*, 459–480.
56. Borghesan, E.C. Giacimenti misti di galene e blende del tipo di metasomatismo di contatto fra intrusione basica e calcare. *Res. Ass. Min. Sarda* **1935**, *40*, 9–13.
57. Cavinato, A. Cenno su un'area metamorfica e sulla genesi e significato di una metallizzazione. *Res. Ass. Min. Sarda* **1937**, *41*, 5–29.
58. ISPRA. Carta Geologica d'Italia Alla Scala 1:50,000. Foglio 556 ASSEMINI. Available online: https://www.isprambiente.gov.it/Media/carg/556_ASSEMINI/Foglio.html (accessed on 16 January 2022).
59. Poll, J.J.K. The Geology of the Rosas-Terraseo area (Sulcis, South Sardinia). *Leidse Geol. Meded.* **1966**, *35*, 117–208.
60. Tearpock, D.J.; Bischke, R.E. *Applied Subsurface Geological Mapping with Structural Methods*, 2nd ed.; Prentice Hall: Upper Saddle River, NJ, USA, 2002; p. 822.

61. Fancello, D.; Deidda, M.L.; Attardi, A.; Cocco, F.; Funedda, A.; Naitza, S. Armenite: A really rare mineral? In Proceedings of the 3rd European Mineralogical Conference EMC, Cracow, Poland, 29 August–2 September 2021; Volume 127.
62. Barton, P.B.; Bethke, P.M. Chalcopyrite disease in sphalerite: Pathology and epidemiology. *Am. Mineral.* **1987**, *72*, 451–467.
63. Poblet, J.; Lisle, R.J. Kinematic evolution and structural styles of fold-and-thrust belts. *Geol. Soc. Lond. Spec. Publ.* **2011**, *349*, 1–24. [[CrossRef](#)]
64. Butler, R.; Bond, C. Chapter 9—Thrust systems and contractional tectonics. In *Regional Geology and Tectonics*, 2nd ed.; Scarselli, N., Adam, J., Chiarella, D., Roberts, D.G., Bally, A.W., Eds.; Elsevier: Amsterdam, The Netherlands, 2020; pp. 149–167. [[CrossRef](#)]
65. Labaume, P.; Sheppard, S.; Moretti, I. Fluid flow in cataclastic thrust fault zones in sandstones, Sub-Andean Zone, Southern Bolivia. *Tectonophysics* **2001**, *340*, 141–172. [[CrossRef](#)]
66. Muñoz-López, D.; Cruset, D.; Cantarero, I.; Benedicto, A.; John, C.M.; Travé, A. Fluid Dynamics in a Thrust Fault Inferred from Petrology and Geochemistry of Calcite Veins: An Example from the Southern Pyrenees. *Geofluids* **2020**, *2020*, 815729. [[CrossRef](#)]
67. Yardley, B.; Warren, C. (Eds.) *An Introduction to Metamorphic Petrology*, 2nd ed.; Cambridge University Press: Cambridge, UK, 2021; Volume 334. [[CrossRef](#)]
68. Del Moro, A.; Di Pisa, A.; Oggiano, G.; Villa, I.M. Isotopic ages of two contrasting tectono-metamorphic episodes in the Variscan chain in northern Sardinia. In Proceedings of the Geologia del Basamento Italiano, Convegno in Memoria di Tommaso Cocozza, Siena, Italy, 21–22 March 1991; Volume 33–35.
69. Dack, A. Internal Structure and Geochronology of the Gerrei Unit in the Flumendosa Area, Variscan External Nappe Zone, Sardinia, Italy. Ph.D. Thesis, Boise State University, Boise, Idaho, 2009; p. 116.
70. Brotzu, P.; Callegari, E.; Secchi, F.A. The search for the parental magma of the high-K calc-alkaline igneous rock series in the southernmost Sardinia Batholith. *Per. Mineral.* **1994**, *62*, 253–280.